mathematics

MDPI

Article

Analytical Treatment of Unsteady Fluid Flow of Nonhomogeneous Nanofluids among Two Infinite Parallel Surfaces: Collocation Method-Based Study

Fengkai Gao [1,†], Dongmin Yu [2,*,†] and Qiang Sheng [3]

[1] School of Electrical Engineering, Northeast Electric Power University, Jilin 132000, China; fk.gao@neepu.edu.cn
[2] School of Information Engineering, Nanchang University, Nanchang 330027, China
[3] School of Sciences, Northeast Electric Power University, Jilin 132000, China; shengqiang0905@163.com
* Correspondence: d.yu@neepu.edu.cn
† Northeast Electric Power University and Nanchang University are in no particular order, and they are the co-first affiliation of this paper.

Abstract: Fluid flow and heat transfer of nanofluids have gained a lot of attention due to their wide application in industry. In this context, the appropriate solution to such phenomena is the study of this exciting and challenging field by the research community. This paper presents an extension of a well-known collocation method (CM) to investigate the accurate solutions to unsteady flow and heat transfer among two parallel plates. First, a mathematical model is developed for the discussed phenomena, then this model is converted into a non-dimensional form using viable similarity variables. In order to inspect the accurate solutions of the accomplished set of nonlinear ordinary differential equations, a collocation method is proposed and applied successfully. Various simulations are performed to analyze the behavior of non-dimensional velocity, temperature, and concentration profiles alongside the deviation of physical parameters present in the model, and then plotted graphically. It is important to mention that the velocity is enhanced due to the higher impact of the parameter *Ha*. The parameter N_t caused an efficient enhancement in the temperature distribution while the parameters N_t provided a drop in the temperature that actually affected the rate of heat transmission. Dual behavior of concentration is noted for parameter *b*, while it can be noted that mixed increasing behavior is available for the concentration against *Le*. The behavior of skin friction, the Nusselt number, and the Sherwood number were also investigated in addition to the physical parameters. It was observed that the Nusselt number increases with the enhancement of the effects of the magnetic field parameter and the Prandtl number. A comparative study shows that the proposed scheme is very effective and reliable in investigating the solutions of the discussed phenomena and can be extended to find the solutions to more nonlinear physical problems with complex geometry.

Keywords: collocation method; squeezing flow; heat transfer; nanofluids

MSC: 65L60; 37C10; 80A05

Citation: Gao, F.; Yu, D.; Sheng, Q. Analytical Treatment of Unsteady Fluid Flow of Nonhomogeneous Nanofluids among Two Infinite Parallel Surfaces: Collocation Method-Based Study. *Mathematics* **2022**, *10*, 1556. https://doi.org/10.3390/math10091556

Academic Editor: James M. Buick

Received: 11 March 2022
Accepted: 30 April 2022
Published: 5 May 2022

1. Introduction

The study of heat transportation and flow analysis is significant due to its appearance in various practical systems, including air-conditioning systems, cooling and heating systems, power generation sector, micro-manufacturing, pharmaceutical processes, transportation, and a few others. The domain of fluid mechanics emerged as an interdisciplinary scientific field of research after a useful innovation by Choi and his team [1]. According to his presented concept, the suspension of small nanoparticles can improve the thermal conductivity that will eventually help improve the heat transfer. Later on, various nanofluid

models were proposed by different researchers, including Buongiorno, Xuan and Li, Tiwari and Das, and Xue and Xu [2–5]. Several research works have been conducted via a similar ideology to study the Navier–Stokes equation using different aspects. Titanium dioxide-shaped nanomaterials have been found to have many useful applications in biological, chemical, and environmental engineering. However, a different nanomaterial has been used to find the performance of heat and flow analysis.

Usman et al. reported a Least-squares method (LSM) approach to inspect the vital impact of thermal conductivity and nonlinear radiation because of the rotatory flow of Copper–Aluminum oxides hybrid nanofluid [6]. In the study, water was used as a base liquid while impacts of bouncy and magnetic forces were considered significant. A comparison was made with the numerical scheme RK-4 to support the solutions of LSM. Hamid et al. studied the role of nanoparticles on the rotatory flow of a nanofluid along a flexible stretching surface [7]. At the same time, a three-shape factor, including brick, platelet, and cylindrical, of molybdenum disulfide (MoS_2) was disclosed. Assumptions were made, including the impacts of magnetic, thermal conductivity, and thermal radiation. The physical system was solved using the concept of the well-known Galerkin approach (GM) and a comparison with existing literature is made to support the mathematical reliability of GM. In another study, heat transport and flow analysis are examined along converging/diverging channels [8]. Two nanoparticles, silver (Ag) and copper (Cu), were used to seek the performance of a proposed model, while water was considered a base liquid. The least-square method was adopted to simulate the proposed model numerically, and outcomes were validated via a comparative study. Mohyud-Din et al. used a modified version of the wavelet approach to examine the heat transfer in rotating nanofluids [9]. In the proposed model, an exponentially stretched surface/sheet was considered. A comparative analysis was made using different nanoparticles, including Silver (Ag), Copper (Cu) and Aluminum (Al_2O_3), Copper (Cu), and Titanium oxide (TiO_2). In another study, Hayat et al. analyzed the mixed convection flow of blood containing Carbon nanotubes (CNTs; both single and multi-wall) over a curved stretching sheet [10]. The nanofluid-based modeling was performed through the concept developed by Xu, while dissipation and Joule heating impacts were incorporated in energy expression.

In addition, the mechanism of fluid motion due to stretching/shirking surfaces or sheets received proper attention. Wang made the pioneer contribution in this regard by exploring the flow next to a stretching surface occupied in the rotatory liquid and used a perturbation-based technique to provide the numerical results of the modeled problem [11]. Later on, several studies were reported in the literature with many different facets. A model study is reported by Yao et al. to analyze the heat transmission through different assets of flows over shrinking/stretching surfaces [12]. Khan and Pop made a pioneer effort to formulate and numerically examine a laminar flow of liquid problem over a stretching sheet and plotted the outcomes through a set of graphs [13]. Shankar et al. reported the impacts of magnetic hydrodynamics polar fluid over a semi-stretching immeasurable perpendicular permeable surface [14]. The model was made by taking the impacts of temperature, heat source, radiation, and magnetic field. The proposed mathematical model was numerically investigated using a hybrid numerical method based on fourth-order Runge–Kutta (RK4) and the shooting technique. The properties of numerous physical parameters on the Nusselt number, skin friction coefficient, and microrotation coefficient were considered, and the conclusions were clarified via a set of plots. Soomro et al. investigated the heat and flow of a non-Newtonian nanofluid along an enlarging surface, while the stagnation point flow of the assumed liquid was taken over a convective shallow [15]. However, the zero normal flux of nanoparticles was measured to scatter the particles away from the surface. Raza et al. offered a numerical study to seek the impacts of the chemical reaction and radiation characteristics in the MHD flow of nanofluids induced by an outwardly elastic diskette taking the effects of a non-uniform heat sink and source [16,17].

It is well-known fact that the squeezing flow mechanism between orthogonally poignant spherical surfaces is involved in various industrial applications. Broadly speak-

ing, squeezing flow comprises synthetic transference in polymer progressions, living body systems, hydro-mechanical machinery, injection, and advances. However, the first contribution towards this phenomenon was made by Stephen, while the same problem using oval and rectangular plates has been studied by Reynold [18,19]. Later on, various authors made various attempts to seek the behavior and analyze it numerically or theoretically. Mohyud-Din et al. adopted a differential transformation technique to examine the heat transposition for the squeezed flow of a non-Newtonian fluid in the equivalent circular plates [20]. Hayat et al. modeled and numerically examined nanofluid's MHD squeezing flow over an external sensor. Three dissimilar types of metal-based nanoparticles alumina, (Al_2O_3), copper (Cu), and titanium dioxide (TiO_2) have been homogeneously incorporated into the water (base liquid) [21]. Haq et al. performed a study that reported an MHD-squeezed stream of a nanofluid over an absorbent elastic sheet/surface. In the study, the induced magnetic field was ignored for minor magnetic Reynolds numbers, and the liquid was electrically led via an applied magnetic field [22]. Chu et al. offered bioconvection features for time-dependent enfolding flow of a non-Newtonian nanofluid with swimming microorganisms over equivalent surfaces in the presence of activation energy and thermal radiation [23]. Waqas et al. modeled a nonhomogeneous nanofluid flow problem and carried out a presentation of the generalized Fick's and Fourier's ideas [24]. The MHD bio-convective features of a couple-stress nanofluid flow over a convective heated elastic sheet with multiple stratified boundary conditions and activation energy. The readers can see further details on more literature on the topic in the references [22,25–35].

The motivation of the current study is to model and examine the nanofluid flow between two substantial analogous plates. The formulated problem is converted to a set of ordinary differential equations using useful similarity approaches. However, the converted version of the problem is tackled via the famous mathematical technique, namely, the collocation method. Additionally, physical performances of included emerging parameters for dimensionless profiles including temperature $g(\eta)$, velocity $f(\eta)$, concentration $h(\eta)$, as well as the physical quantities Sherwood number, local Nusselt number, and skin friction coefficient, have been expressed via graphical plots. It is worthy to mention that the velocity is enhanced due to the higher impact of the parameter Ha (Hartmann number), while a different kind of behavior, actually a drop, is provided by the parameter f_0. The parameter N_t caused an efficient enhancement in the temperature distribution, while the parameters N_t and f_0 provided a drop in the temperature that actually affected the rate of heat transmission. Dual behavior of concentration is noted for parameter b, while it can be noted that mixed increasing behavior is available for the concentration against Le. The concentration and velocity profiles dropped due to the increasing values of parameter b, but the impact of parameter b is more significant on concentration. It showed a dual behavior for concentration after a particular stretch. The proposed methodology was found to be really effective to deal with nonlinear mechanical or fluid dynamical problems. These kinds of methods can be further used for a class of nonlinear problems arising in mechanics [36–41].

The manuscript is organized as a literature survey, and a brief introduction is reported in the first section. In Section 2, the mathematical and physical structure of the problem is explained. The detailed methodology of the collocation method is given in Section 3. Section 4 is devoted to performing a detailed analysis, results, and physical discussion of the proposed model. Section 5 is devoted to conclusions.

2. Mathematical Modeling

Assume that the unsteady fluid flow, heat, and mass transfer among the two plates are parallel in direction. The plates are bounded inside a squeezing channel. Consider the free stream squeezing flow, which begins from the tip of the plate, while the altitude $h(t)$ is larger than the thickness of the boundary layer. There is no applied electric field and the magnetic Reynolds number is very small, and, hence, the induced magnetic field is neglected. Hall impact was also neglected. It is also considered that there is a microcantilever sensor

between the two parallel plates, where the upper plate is squeezed and the lower plate is immovable, as shown in Figure 1. Keeping in mind these assumptions, the physical model of the fluid flow, heat, and mass transfer is given as [6–8]:

$$\frac{\partial U}{\partial x} + \frac{\partial V}{\partial y} = 0, \tag{1}$$

$$\frac{\partial U}{\partial t} + U\frac{\partial U}{\partial x} + V\frac{\partial U}{\partial y} = -\frac{\sigma B^2}{\rho}U - \frac{1}{\rho}\frac{\partial p}{\partial x} + \frac{\mu}{\rho}\frac{\partial^2 U}{\partial y^2}, \tag{2}$$

$$\frac{\partial u}{\partial t} + U\frac{\partial u}{\partial x} = -\frac{1}{\rho}\frac{\partial p}{\partial x} - \frac{\sigma B^2}{\rho}u, \tag{3}$$

$$\frac{\partial \Theta}{\partial t} + U\frac{\partial \Theta}{\partial x} + V\frac{\partial \Theta}{\partial y} = \alpha\frac{\partial^2 \Theta}{\partial x^2} + \tau\left[D_B\frac{\partial \Phi}{\partial y}\frac{\partial \Theta}{\partial y} + \frac{D_T}{T_\infty}\left(\frac{\partial \Theta}{\partial y}\right)^2\right], \tag{4}$$

$$\frac{\partial \Phi}{\partial t} + U\frac{\partial \Phi}{\partial x} + V\frac{\partial \Phi}{\partial y} = D_B\frac{\partial^2 \Phi}{\partial y^2} + \frac{D_T}{T_\infty}\frac{\partial^2 \Theta}{\partial y^2}. \tag{5}$$

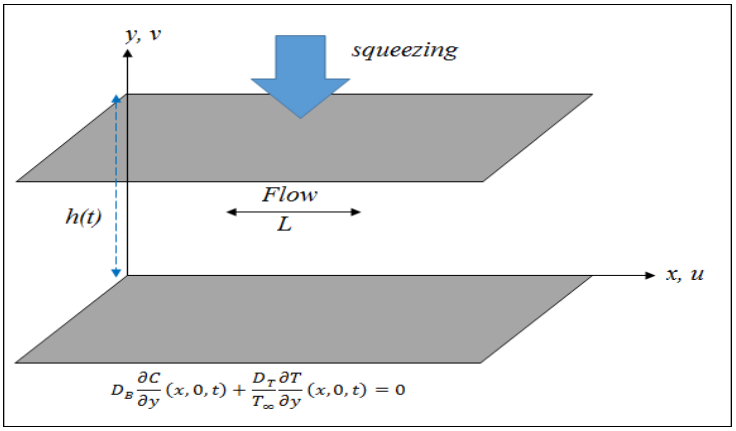

Figure 1. Systematic diagram of the governing model.

In Equations (1)–(5), U and V are represented by the velocity components horizontal and normal respectively. Moreover, u indicates the free stream velocity, Θ denotes the temperature of the fluid, t is represented by time, B shows the magnetic field effect, pressure is denoted by p, μ specifies the kinematic viscosity, ρ is denoted by density, the concentration of the fluid is presented by Φ, and D_B and D_T are the Brownian and thermophoresis diffusion, respectively. The boundary conditions associated with the discussed problem are given as:

$$U = D_B\frac{\partial \Phi}{\partial y} + \frac{D_T}{T_\infty}\frac{\partial \Theta}{\partial y} = 0, V = V_0(t), -k\frac{\partial \Theta}{\partial y} = q(x), \text{ at } y = 0, \tag{6}$$

$$U = u(x,t), \Theta = \Theta_\infty, \Phi = \Phi_\infty, \text{ at } y \to \infty. \tag{7}$$

We obtained the following equation after equating Equations (2) and (3) as:

$$\frac{\partial U}{\partial t} + U\frac{\partial U}{\partial x} + V\frac{\partial U}{\partial y} = \frac{\partial u}{\partial t} + U\frac{\partial u}{\partial x} + \frac{\mu}{\rho}\frac{\partial^2 U}{\partial y^2} - \frac{\sigma B^2}{\rho}(U - u), \tag{8}$$

In Equations (6) and (7), $u(x,t)$ and Θ_∞ denote the free stream velocity and temperature, respectively; however, $q(x)$ signifies the heat flux, and $V_0(t)$ specifies the velocity at

the sensor surface. Consider the following similarity variables to convert the governing model (4)–(8) into non-dimensional form as:

$$f(\eta) = \frac{\psi}{x\sqrt{av}},\ g(\eta) = k\frac{\Theta - \Theta_\infty}{q_0 x\sqrt{\nu/a}},\ h = \frac{\Phi - \Phi_\infty}{\Phi_w - \Phi_\infty},\ \eta = y\sqrt{\frac{a}{\nu}}, u = ax,\ a = \frac{1}{s+bt}. \quad (9)$$

We obtained the following dimensionless set of nonlinear ordinary differential equations after applying the similarity variables (9) as:

$$f'''(\eta) + \left(f(\eta) + \frac{b}{2}\eta\right)f'' - \left(f'(\eta)\right)^2 + b\left(f'(\eta) - 1\right) - Ha\left(f'(\eta) - 1\right) + 1 = 0, \quad (10)$$

$$\frac{1}{\mathrm{Pr}}g''(\eta) + \left(f + \frac{b}{2}\eta\right)g'(\eta) + \left(f' + \frac{b}{2}\right)g(\eta) + N_b g'(\eta)h'(\eta) + N_t\left(g'(\eta)\right)^2 = 0, \quad (11)$$

$$h''(\eta) + \mathrm{Pr}Le\left(f(\eta) + \frac{b}{2}\eta\right)h'(\eta) + \frac{N_t}{N_b}g''(\eta) = 0. \quad (12)$$

After applying the similarity variables (9), the dimensionless conditions given in Equations (6) and (7) are transformed into the following form:

$$\text{For } \eta = 0, \qquad f(\eta) = f_0,\ f'(\eta) = 0,\ g'(\eta) = -1,\ N_b h'(\eta) + N_b g'(\eta) = 0, \quad (13)$$

$$\text{When } \eta \to \infty, \qquad f'(\eta) = 1, g(\eta) = h(\eta) = 0, \quad (14)$$

where Ha shows the Hartmann number, b indicates the squeezed parameter, Pr is represented by the Prandtl number, N_t andf N_b are the thermophoretic and Brownian motion parameters, respectively, Le signifies the Lewis number, and f_0 presents the permeable velocity parameter. Dimensionless Skin friction, and the Nusselt and Sherwood numbers are defined as:

$$C_{fx} = \frac{\tau_w}{a\mathrm{Re}^{1/2}} = f''(0),\ \mathrm{Re}^{-1/2}Nu = -g'(0),\ \mathrm{Re}^{-\frac{1}{2}}Sh = -h'(0). \quad (15)$$

The above local Reynolds parameter is indicated as $\mathrm{Re}_x = ax^2/\nu$.

3. Solution Procedure via CM

This section is dedicated to developing the collocation method for the numerical solution of unsteady flow of nanofluids and heat transfer among plates (10)–(14). This method is very simple and based on collocation points and used for the numerical treatment of fluid flow and heat transfer of human blood with nanoparticles over permeable vessels, flow and heat moving of ferrofluids beside a smooth surface, and free bio-convection fluid flow of nanofluids in three dimensions close to a stagnation point and highly nonlinear oscillatory fractional-order differential models [42–46]. In this work, the authors prove that the collocation method is stable and convergent both numerically as well as theoretically. A step-by-step explanation of this method is given as:

Step 1: In this scheme, first of all, we consider the non-dimensional form (10)–(14) of the governing model (1)–(7) as:

$$f'''(\eta) + \left(f(\eta) + \frac{b}{2}\eta\right)f'' - \left(f'(\eta)\right)^2 + b\left(f'(\eta) - 1\right) - Ha\left(f'(\eta) - 1\right) + 1 = 0, \quad (16)$$

$$\frac{1}{\mathrm{Pr}}g''(\eta) + \left(f + \frac{b}{2}\eta\right)g'(\eta) + \left(f' + \frac{b}{2}\right)g(\eta) + N_b g'(\eta)h'(\eta) + N_t\left(g'(\eta)\right)^2 = 0, \quad (17)$$

$$h''(\eta) + \mathrm{Pr}Le\left(f(\eta) + \frac{b}{2}\eta\right)h'(\eta) + \frac{N_t}{N_b}g''(\eta) = 0. \quad (18)$$

Step 2: In this collocation strategy, the estimate of the solutions of the velocity profile $f(\eta)$ is denoted by $\widetilde{f}(\eta)$, temperature distribution $g(\eta)$ is represented by $\widetilde{g}(\eta)$, and concentration profile $h(\eta)$ is specified by $\widetilde{h}(\eta)$ and given as a finite sum with the help of constants as prescribe as under:

$$\widetilde{f}(\eta) = \vartheta_0^1 + \vartheta_1^1\eta + \vartheta_2^1\eta^2 + \ldots + \vartheta_N^1\eta^N = \sum_{k=0}^{N} \vartheta_k^1\eta^k, \tag{19}$$

$$\widetilde{g}(\eta) = \vartheta_0^2 + \vartheta_1^2\eta + \vartheta_2^2\eta^2 + \ldots + \vartheta_N^2\eta^N = \sum_{k=0}^{N} \vartheta_k^2\eta^k, \tag{20}$$

$$\widetilde{h}(\eta) = \vartheta_0^3 + \vartheta_1^3\eta + \vartheta_2^3\eta^2 + \ldots + \vartheta_N^3\eta^N = \sum_{k=0}^{N} \vartheta_k^3\eta^k. \tag{21}$$

Here, in the above trial solutions (19)–(21), N signifies the order of approximation, typically known as the convergence control parameter and $\vartheta_k^1,\ \vartheta_k^2,\ \vartheta_k^3$ for $k = 0, 1, 2, \ldots, N$ are the unknown constants that need to be investigated. Since, in the collocation method, the trial solutions (19)–(21) need to fulfill the boundary conditions, after applying the boundary conditions (13) and (14), the trial solutions (19)–(21) are shrunk as:

$$\widetilde{f}(\eta) = -f_0 + \frac{1}{2\eta_\infty}\eta^2 + \sum_{k=3}^{N} \vartheta_k^1\left[\eta^{k-2} - \frac{k}{2}\eta_\infty^{k-2}\right]\eta^2, \tag{22}$$

$$\widetilde{g}(\eta) = -\eta + \eta_\infty + \sum_{k=2}^{N} \vartheta_k^2[\eta^n - \eta_\infty^n], \tag{23}$$

$$\widetilde{h}(\eta) = -(\eta + \eta_\infty)\frac{N_t}{N_b}\widetilde{g}(0) + \sum_{k=2}^{N} \vartheta_k^3[\eta^n - \eta_\infty^n]. \tag{24}$$

Step 3: The residual functions of $f(\eta)$, $g(\eta)$ and $h(\eta)$ are as given below after replacing the trial solutions (22)–(24) into Equations (16)–(18):

$$\begin{aligned} R_f\left(\eta, \vartheta_l^1, \vartheta_m^2, \vartheta_n^3\right) = \widetilde{f}'''(\eta) + \left(\widetilde{f}(\eta) + \tfrac{b}{2}\eta\right)\widetilde{f}''(\eta) - \left(\widetilde{f}'(\eta)\right)^2 + b\left(\widetilde{f}'(\eta) - 1\right) \\ -Ha\left(\widetilde{f}'(\eta) - 1\right) + 1 \neq 0, \end{aligned} \tag{25}$$

$$\begin{aligned} R_g\left(\eta, \vartheta_l^1, \vartheta_m^2, \vartheta_n^3\right) = \tfrac{1}{\mathrm{Pr}}\widetilde{g}''(\eta) + \left(\widetilde{f}(\eta) + \tfrac{b}{2}\eta\right)\widetilde{g}'(\eta) + \left(\widetilde{f}'(\eta) + \tfrac{b}{2}\right)\widetilde{g}(\eta) \\ +N_b\widetilde{g}'(\eta)\widetilde{h}'(\eta) + N_t(\widetilde{g}'(\eta))^2 \neq 0, \end{aligned} \tag{26}$$

$$R_h\left(\eta, \vartheta_l^1, \vartheta_m^2, \vartheta_n^3\right) = \widetilde{h}''(\eta) + \mathrm{Pr}Le\left(\widetilde{f}(\eta) + \frac{b}{2}\eta\right)\widetilde{h}'(\eta) + \frac{N_t}{N_b}\widetilde{g}''(\eta) \neq 0. \tag{27}$$

Step 4: We have only three algebraic equations R_f, R_g, and R_h and $(N-2)(N-1)$ $(N-1)$ number of unknowns; therefore, in order to find the unique solution, we must have $(N-2)(N-1)(N-1)$ number of algebraic equations. Thus, we can use the collocation technique and collocate the above residual functions (25)–(27) at the following equal spaced collocation points:

$$\eta = \eta_k = \frac{k}{N},\ k = 1, 2, 3, 4, \ldots, N.$$

Step 5: After solving the above nonlinear system of algebraic equations that were attained in step 4, we obtained the numerical values of unknown constants by setting these unknowns into the trial solutions (22)–(24), to obtain accurate solutions of the discussed problem.

4. Results and Discussion

Unsteady fluid flow, heat, and mass transfer between two surfaces were carried out using the well-known collocation approach. This segment is committed to inspecting the influence of the non-dimensional physical parameters including the Prandtl number, Hartmann number, unsteady parameter, etc., on the dimensionless velocity "$f(\eta)$", temperature "$h(\eta)$", and concentration "$h(\eta)$" profiles with the help of graphs (see Figures 1–3) and comprehensive argument (see Tables 1 and 2). Figure 4 and Table 3 show the comparative analysis.

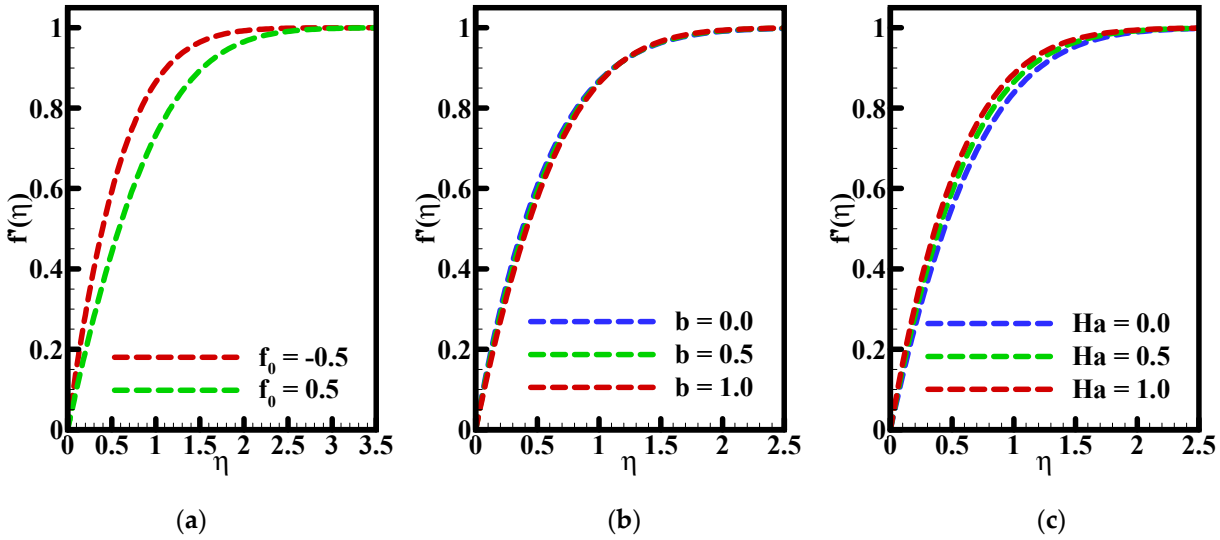

Figure 2. Impact of the parameters (**a**) f_0, (**b**) b, and (**c**) Magnetic parameter (Ha) on the dimensionless velocity profile and numerous choices of emerging parameters.

Table 1. The behavior of the physical quantities of skin friction, the Nusselt number, and the Sherwood number under the variation in physical parameters.

M	b	f_0	Pr	N_t	N_b	Le	$f''(0)$	$\frac{1}{g(0)}$	$h'(0)$
0	0.5	−0.5	3.97	0.3	0.5	2	1.41209	0.53992	-
1	-	-	-	-	-	-	1.60239	0.55369	-
2	-	-	-	-	-	-	1.77102	0.56518	-
0.5	0	-	-	-	-	-	1.71854	0.45771	-
-	0.5	-	-	-	-	-	1.60239	0.55370	-
-	1	-	-	-	-	-	1.48114	0.67073	-
-	0.25	−0.5	-	-	-	-	1.66109	0.50362	-
-	-	0.5	-	-	-	-	1.09294	−0.22818	-
-	-	−0.5	3	-	-	-	-	0.48136	-
-	-	-	5	-	-	-	-	0.53414	-
-	-	-	7	-	-	-	-	0.59050	-
-	-	-	6.2	0.1	-	-	-	2.86340	0.2000
-	-	-	-	0.2	-	-	-	0.35443	0.4000
-	-	-	-	0.3	-	-	-	0.56881	0.6000
-	-	-	-	0.3	0.1	-	-	-	3.0000
-	-	-	-	-	0.2	-	-	-	1.5000
-	-	-	-	-	0.3	-	-	-	1.0000
-	-	-	-	-	0.5	0	-	3.09699	-
-	-	-	-	-	-	2	-	0.56881	-
-	-	-	-	-	-	5	-	0.65213	-

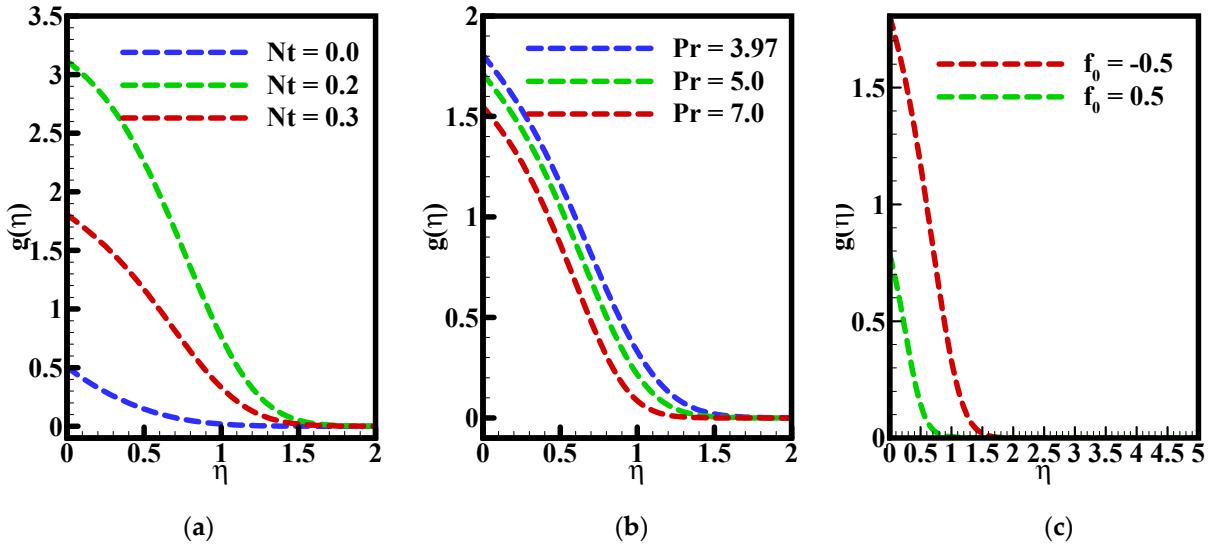

Figure 3. Influence of the parameters (**a**) Nt, (**b**) Prandtl number (Pr), and (**c**) f_0 on the dimensionless temperature distribution and numerous choices of emerging parameters.

Table 2. Velocity, temperature, and concentration profile vary the η by taking different values of prominent parameters.

η	Veclocity	Temperature	Concentration
0.00	0.00000000	1.80602974	−0.11719518
0.30	0.40286279	1.46945390	0.00092259
0.60	0.66809369	0.99463258	0.06836315
0.90	0.82887854	0.47417323	0.08077955
1.20	0.91848603	0.13083488	0.04128107
1.50	0.96427592	0.01941746	0.00878368
1.80	0.98566979	0.00170315	0.00088685
2.10	0.99478720	0.00009441	0.00005156
2.40	0.99832789	0.00000335	0.00000187
2.70	0.99958484	0.00000007	0.00000004
3.00	1.00000000	0.00000000	0.00000000

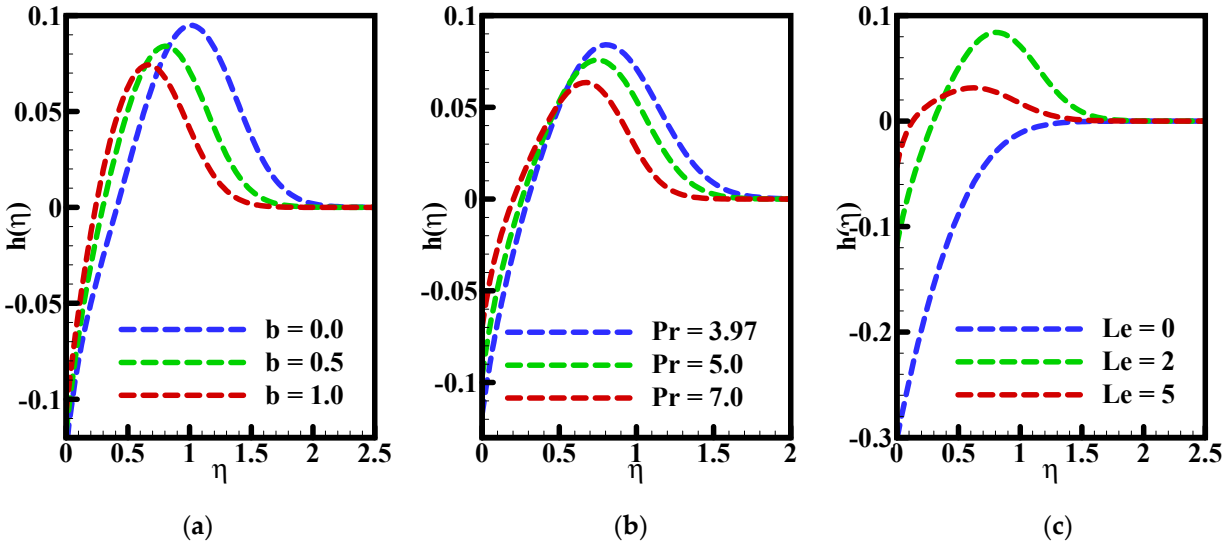

Figure 4. Effect of the parameters (**a**) b, (**b**) Prandtl number (Pr), and (**c**) Lewin number (Le) on the dimensionless concentration profile and numerous choices of emerging parameters.

Table 3. Comparisons of the values of $-f''(0)$ obtained via the proposed scheme with existing results [41–46] against various values of b.

$-b$	[47]	[48]	[49]	[50]	[51]	[52]	Present
0.0	-	-	-	1.0005	1.00000	1.00000	1.00000
0.2	-	-	-	1.0685	1.06874	1.06801	1.06871
0.4	-	-	-	1.1349	1.13521	1.13469	1.13522
0.6	-	-	-	1.1992	1.19930	1.19912	1.19924
0.8	1.261512	1.26104	1.261479	-	1.26099	1.26104	1.26092
1.2	1.378052	1.37772	1.377850	-	1.37755	1.37772	1.37761
2.0	-	-	-	-	1.58740	1.58737	1.58738

Simulations were performed for $N = 25$ and the values of parameters were taken as $f_0 = -0.5$, $b = 0.5, \Pr = 3.97$, $Ha = 0.5$, $N_t = 0.3$, $N_b = 0.5$, and $Le = 2$. In Figure 2a–c, the impact of the different parameters, including f_0, b, and Ha, on the dimensionless velocity is illustrated. In Figure 2a, the influence of parameter f_0 on velocity is analyzed and plotted graphically. It can be seen from Figure 2a that changing the values of f_0 is produced a drop in the performance of velocity. In Figure 2b, the impacts of parameter b are illustrated where a minor drop in the velocity is noted for higher values of parameter b. It is clear from the graphical designs that the impact of the parameter is unimportant. The parameter Ha is a magnetic number causing an improvement in the velocity profile, where increasing the value of the Hartmann number (Ha) produces an increase in the velocity. It is expected that since a decrease in the Hartmann number yields an increase in the dynamic viscosity, and if the viscosity of the fluid increases, the flow of the fluid decreases; in other words, the velocity profile decreases. The behavior of the temperature profile through different parameter variations is illustrated in Figure 3a–c. The parameter N_t causes an increase in the temperature, which means it provides a better rate of heat transfer and is available in Figure 3a. Figure 3b displays the behavior of temperature against an increase in the parameter Pr. It shows that a drop in the temperature profile increases the values of the Pr parameter. Physically, it is true, since the Prandtl number is inversely proportional to the thermal diffusivity of the fluid, and enlargement of the Prandtl number leads to a drop in thermal diffusivity that ultimately yields to a drop in the temperature profile. A drop in the temperature is noted when the value of parameter f_0 is displayed, as in Figure 3c. The analysis of the concentration profile for parameters b, Pr, and Le is displayed in Figure 4a–c. Dual behavior of concentration is noted for parameter b, which is displayed in Figure 4a. In Figure 4b, values of Pr are increased, and the concentration behavior is graphically checked. It is noticed that a twin-type concentration profile is available when increasing Pr. However, the other brand is more dominantly dropped than in the first half of the branch where an increase is observed, but a minor impactful increase is noticed. The impact of Le on concentration is graphically displayed in Figure 4c, where it can be seen that mixed increasing behavior is available for the concentration against Le. It is also expected physically. The behavior of the skin friction coefficient and the local Nusselt number in varying the physical parameters are also deliberated in tabular form. The method is validated for different ranges of parameters, and a comparison is available in Table 1. It is important to mention that the skin friction coefficient increases against the variation in the Hartmann number and decreases against the variation in b and f_0. The local Nusselt number demonstrates the increasing behavior as enhancing Ha, b, and Pr, and demonstrates the decreasing behavior as varying f_0, N_t, and L_e. Table 2 is presented to show the solutions obtained by the collocation scheme and it is found relatively easily compared with the other mathematical methods. Figure 5 and Table 3 are constructed to see the effectiveness of the proposed algorithms. It is interesting to point out that the suggested schemes give very accurate results as compared to the fourth-order Runge–Kutta schemes and existing results [47–49].

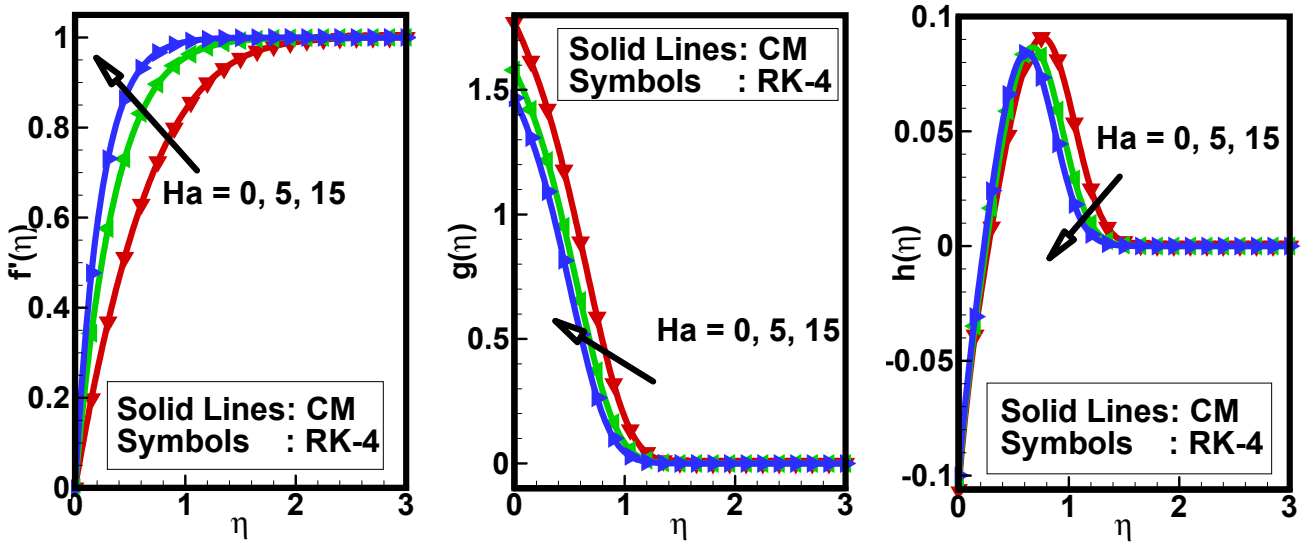

(**a**) (**b**) (**c**)

Figure 5. Comparison between the obtained solution with the collocation method (CM) and fourth-order Runge–Kutta (RK-4) of the dimensionless (**a**) velocity, (**b**) temperature, and (**c**) concentration profiles as varying *Ha*.

5. Conclusions

In this article, a mathematical model of unsteady fluid flow, heat, and mass transfer among two parallel plates is developed. Viable similarity variables are suggested and used to transform the governing set of partial differential equations into a set of nonlinear dimensionless ordinary differential equations. Next, a collocation scheme is extended and magnificently used to investigate the accurate solutions of the obtained set of nonlinear dimensionless ordinary differential equations. Various simulations have been executed for the performance of non-dimensional velocity f', temperature g, and concentration h profiles beside the physical parameters.

- The velocity is enhanced due to the higher impact of the parameter H_a (Hartmann number), while a different kind of behavior, actually a drop, is provided by the parameter f_0.
- The parameter N_t caused an efficient enhancement in the temperature distribution, while the parameters N_t and f_0 provided a drop in the temperature that actually affected the rate of heat transmission.
- Dual behavior of concentration is noted for parameter b, while it can be noted that mixed increasing behavior is available for the concentration against L_e.
- The concentration and velocity profiles dropped due to the increasing values of parameter b, but the impact of parameter b is more significant on concentration. It showed a dual behavior for concentration after a particular stretch.
- It is observed that the proposed methodology is found to be really effective to deal with nonlinear mechanical or fluid dynamical problems.
- The presented method can be further used for a class of nonlinear problems arising in mechanics.
- The proposed scheme can be extended to investigate the solution of channel flow, fractional-order fluid flow, unsteady cavity models, etc.

Author Contributions: Conceptualization, methodology, validation, formal analysis, investigation, resources, data curation, writing—original draft preparation, writing—review and editing, visualization, supervision, project administration and funding acquisition, F.G., D.Y. and Q.S. All authors have read and agreed to the published version of the manuscript."

Funding: This research was funded by Nanchang University.

Institutional Review Board Statement: Not applicable.

Informed Consent Statement: Not applicable.

Data Availability Statement: Not applicable.

Conflicts of Interest: The authors declare no conflict of interest.

Nomenclature

$h(t)$	Distance between two plates
U and V	Velocity components in x- and y-directions
u	Free stream velocity
Θ	Temperature of the fluid
C	Concentration of the fluid
B	Magnetic field
p	Pressure
μ	Kinematic viscosity
ρ	Density
D_B	Brownian parameter
D_T	Thermophoresis diffusion parameter
Θ_∞	Free stream temperature
$q(x)$	Heat flux
$V_0(t)$	Velocity at sensor surface
Ha	Hartmann number
b	Squeezed parameter
Pr	Prandtl number
N_t	Thermophoretic parameter
N_b	Brownian motion parameter
Le	Lewis number
f_0	Permeable velocity
Re	Local Reynolds number
CM	Collocation method

References

1. Choi, S.U.; Eastman, J.A. *Enhancing Thermal Conductivity of Fluids with Nanoparticles*; Argonne National Lab.: Lemont, IL, USA, 1995.
2. Buongiorno, J. Convective transport in nanofluids. *J. Heat Transf.* **2006**, *128*, 240–250. [CrossRef]
3. Xuan, Y.; Li, Q. Heat transfer enhancement of nanofluids. *Int. J. Heat Fluid Flow* **2000**, *21*, 58–64. [CrossRef]
4. Tiwari, R.K.; Das, M.K. Heat transfer augmentation in a two-sided lid-driven differentially heated square cavity utilizing nanofluids. *Int. J. Heat Mass Transf.* **2007**, *50*, 2002–2018. [CrossRef]
5. Xue, Q.; Xu, W.-M. A model of thermal conductivity of nanofluids with interfacial shells. *Mater. Chem. Phys.* **2005**, *90*, 298–301. [CrossRef]
6. Usman, M.; Hamid, M.; Zubair, T.; Haq, R.U.; Wang, W. Cu-Al2O3/Water hybrid nanofluid through a permeable surface in the presence of nonlinear radiation and variable thermal conductivity via LSM. *Int. J. Heat Mass Transf.* **2018**, *126*, 1347–1356. [CrossRef]
7. Hamid, M.; Usman, M.; Zubair, T.; Haq, R.U.; Wang, W. Shape effects of MoS2 nanoparticles on rotating flow of nanofluid along a stretching surface with variable thermal conductivity: A Galerkin approach. *Int. J. Heat Mass Transf.* **2018**, *124*, 706–714. [CrossRef]
8. Usman, M.; Haq, R.U.; Hamid, M.; Wang, W. Least square study of heat transfer of water based Cu and Ag nanoparticles along a converging/diverging channel. *J. Mol. Liq.* **2018**, *249*, 856–867. [CrossRef]
9. Mohyud-Din, S.T.; Hamid, M.; Usman, M.; Kanwal, A.; Zubair, T.; Wang, W.; Nazir, A. Rotating flow of nanofluid due to exponentially stretching surface: An optimal study. *J. Algorithms Comput. Technol.* **2019**, *13*, 1748302619881365. [CrossRef]

10. Hayat, T.; Khan, S.A.; Alsaedi, A.; Zai, Q.Z. Computational analysis of heat transfer in mixed convective flow of CNTs with entropy optimization by a curved stretching sheet. *Int. Commun. Heat Mass Transf.* **2020**, *118*, 104881. [CrossRef]
11. Wang, C. Stretching a surface in a rotating fluid. *Z. Angew. Math. Und Phys. ZAMP* **1988**, *39*, 177–185. [CrossRef]
12. Yao, S.; Fang, T.; Zhong, Y. Heat transfer of a generalized stretching/shrinking wall problem with convective boundary conditions. *Commun. Nonlinear Sci. Numer. Simul.* **2011**, *16*, 752–760. [CrossRef]
13. Khan, W.; Pop, I. Boundary-layer flow of a nanofluid past a stretching sheet. *Int. J. Heat Mass Transf.* **2010**, *53*, 2477–2483. [CrossRef]
14. Bejawada, S.G.; Khan, Z.H.; Hamid, M. Heat generation/absorption on MHD flow of a micropolar fluid over a heated stretching surface in the presence of the boundary parameter. *Heat Transf.* **2021**, *50*, 6129–6147. [CrossRef]
15. Soomro, F.A.; Haq, R.U.; Khan, Z.H.; Zhang, Q. Passive control of nanoparticle due to convective heat transfer of Prandtl fluid model at the stretching surface. *Chin. J. Phys.* **2017**, *55*, 1561–1568. [CrossRef]
16. Naqvi, S.M.R.S.; Muhammad, T.; Saleem, S.; Kim, H.M. Significance of non-uniform heat generation/absorption in hydromagnetic flow of nanofluid due to stretching/shrinking disk. *Phys. A Stat. Mech. Its Appl.* **2020**, *553*, 123970. [CrossRef]
17. Fan, S.; Wang, Y.; Cao, S.; Zhao, B.; Sun, T.; Liu, P. A deep residual neural network identification method for uneven dust accumulation on photovoltaic (PV) panels. *Energy* **2022**, *239*, 122302. [CrossRef]
18. Stefen, M. Versuch Uber die scheinbare adhesion. *Sitz. Akad. Wiss. Wien Math. Nat.* **1874**, *69*, 713–721.
19. Reynolds, O.I.V. On the theory of lubrication and its application to Mr. Beauchamp tower's experiments, including an experimental determination of the viscosity of olive oil. *Philos. Trans. R. Soc. Lond.* **1886**, *177*, 157–234.
20. Mohyud-Din, S.T.; Usman, M.; Wang, W.; Hamid, M. A study of heat transfer analysis for squeezing flow of a Casson fluid via differential transform method. *Neural Comput. Appl.* **2018**, *30*, 3253–3264. [CrossRef]
21. Hayat, T.; Muhammad, T.; Qayyum, A.; Alsaedi, A.; Mustafa, M. On squeezing flow of nanofluid in the presence of magnetic field effects. *J. Mol. Liq.* **2016**, *213*, 179–185. [CrossRef]
22. Haq, R.U.; Nadeem, S.; Khan, Z.H.; Noor, N.F. MHD squeezed flow of water functionalized metallic nanoparticles over a sensor surface. *Phys. E Low-Dimens. Syst. Nanostruct.* **2015**, *73*, 45–53. [CrossRef]
23. Chu, Y.M.; Khan, M.I.; Waqas, H.; Farooq, U.; Khan, S.U.; Nazeer, M. Numerical simulation of squeezing flow Jeffrey nanofluid confined by two parallel disks with the help of chemical reaction: Effects of activation energy and microorganisms. *Int. J. Chem. React. Eng.* **2021**, *19*, 717–725. [CrossRef]
24. Waqas, H.; Wakif, A.; Al-Mdallal, Q.; Zaydan, M.; Farooq, U. Significance of magnetic field and activation energy on the features of stratified mixed radiative-convective couple-stress nanofluid flows with motile microorganisms. *Alex. Eng. J.* **2021**, *61*, 1425–1436. [CrossRef]
25. Munawar, S.; Mehmood, A.; Ali, A. Three-dimensional squeezing flow in a rotating channel of lower stretching porous wall. *Comput. Math. Appl.* **2012**, *64*, 1575–1586. [CrossRef]
26. Li, F.; Soomro, F.A.; Imtiaz, J. Influences of imposed magnetic force on treatment of hybrid nanofluid involving non-Darcy porous model. *Int. Commun. Heat Mass Transf.* **2021**, *125*, 105318. [CrossRef]
27. Usman, M.; Zubair, T.; Hamid, M.; Haq, R.U.; Khan, Z.H. Unsteady flow and heat transfer of tangent-hyperbolic fluid: Legendre wavelet-based analysis. *Heat Transf.* **2021**, *50*, 3079–3093. [CrossRef]
28. Nayak, M.K.; Akbar, N.S.; Pandey, V.S.; Khan, Z.H.; Tripathi, D. 3D free convective MHD flow of nanofluid over permeable linear stretching sheet with thermal radiation. *Powder Technol.* **2017**, *315*, 205–215. [CrossRef]
29. Hussain, S.; Khan, Z.; Nadeem, S. Water driven flow of carbon nanotubes in a rotating channel. *J. Mol. Liq.* **2016**, *214*, 136–144. [CrossRef]
30. Fan, S.; Wang, Y.; Cao, S.; Sun, T.; Liu, P. A novel method for analyzing the effect of dust accumulation on energy efficiency loss in photovoltaic (PV) system. *Energy* **2021**, *34*, 121112. [CrossRef]
31. Haq, R.U.; Hammouch, Z.; Khan, W.A. Water-based squeezing flow in the presence of carbon nanotubes between two parallel disks. *Therm. Sci.* **2016**, *20*, 1973–1981. [CrossRef]
32. Khan, Z.H.; Usman, M.; Zubair, T.; Hamid, M.; Haq, R.U. Brownian motion and thermophoresis effects on unsteady stagnation point flow of Eyring–Powell nanofluid: A Galerkin approach. *Commun. Theor. Phys.* **2020**, *72*, 125005. [CrossRef]
33. Usman, M.; Mohyud Din, S.T.; Zubair, T.; Hamid, M.; Wang, W. Fluid flow and heat transfer investigation of blood with nanoparticles through porous vessels in the presence of magnetic field. *J. Algorithms Comput. Technol.* **2018**, *13*, 1748301818788661. [CrossRef]
34. Ghalambaz, M.; Groşan, T.; Pop, I. Mixed convection boundary layer flow and heat transfer over a vertical plate embedded in a porous medium filled with a suspension of nano-encapsulated phase change materials. *J. Mol. Liq.* **2019**, *293*, 111432. [CrossRef]
35. Mehryan, S.A.M.; Izadpanahi, E.; Ghalambaz, M.; Chamkha, A.J. Mixed convection flow caused by an oscillating cylinder in a square cavity filled with Cu–Al2O3/water hybrid nanofluid. *J. Therm. Anal. Calorim.* **2019**, *137*, 965–982. [CrossRef]
36. Yang, S.; Tan, J.; Chen, B. Robust Spike-Based Continual Meta-Learning Improved by Restricted Minimum Error Entropy Criterion. *Entropy* **2022**, *24*, 455. [CrossRef]
37. Li, P.; Gao, X.; Li, Z.; Zhou, X. Effect of the temperature difference between land and lake on photovoltaic power generation. *Renewable Energy* **2022**, *185*, 86–95. [CrossRef]
38. Huang, L.; Zhou, W.; Xu, H.; Wang, L.; Zou, J.; Zhou, Q. Dynamic fluid states in organic-inorganic nanocomposite: Implications for shale gas recovery and CO2 sequestration. *Chem. Eng. J.* **2021**, *411*, 128423. [CrossRef]

39. Zhu, T.; Li, Q.; Yu, A. Analysis of the solar spectrum allocation in a spectral-splitting photovoltaic-thermochemical hybrid system. *Solar Energy* **2022**, *232*, 63–72. [CrossRef]
40. Guo, Z.; Yang, J.; Tan, Z.; Tian, X.; Wang, Q. Numerical study on gravity-driven granular flow around tube out-wall: Effect of tube inclination on the heat transfer. *Int. J. Heat Mass Transf.* **2020**, *174*, 121296. [CrossRef]
41. Cai, T.; Dong, M.; Liu, H.; Nojavan, S. Integration of hydrogen storage system and wind generation in power systems under demand response program: A novel p-robust stochastic programming. *Int. J. Hydrogen Energy* **2021**, *47*, 443–458. [CrossRef]
42. Usman, M.; Hamid, M.; Mohyud Din, S.T.; Waheed, A.; Wang, W. Exploration of uniform heat flux on the flow and heat transportation of ferrofluids along a smooth plate: Comparative investigation. *Int. J. Biomath.* **2018**, *11*, 1850048. [CrossRef]
43. Usman, M.; Hamid, M.; Rashidi, M.M. Gegenbauer wavelets collocation-based scheme to explore the solution of free bio-convection of nanofluid in 3D nearby stagnation point. *Neural Comput. Appl.* **2019**, *31*, 8003–8019. [CrossRef]
44. Yu, D.; Zhao, X.; Wang, Y.; Jiang, L.; Liu, H. Research on Energy Management of a Virtual Power Plant Based on the Improved Cooperative Particle Swarm Optimization Algorithm. *Front. Energy Res.* **2022**, *10*, 785569. [CrossRef]
45. Hamid, M.; Usman, M.; Haq, R.U.; Tian, Z. A spectral approach to analyze the nonlinear oscillatory fractional-order differential equations. *Chaos Solitons Fractals* **2021**, *146*, 110921. [CrossRef]
46. Zaheer, M.; Khan, H.; Shah, S.H.; Mashwani, S.A.; ul Haq, E.; Manzoor, F. Solute transport modelling in low-permeability homogeneous and saturated soil media: Transport in low-permeability soil media. *Rud.-Geološko-Naft. Zb. (Min. Geol. Pet. Bull.)* **2021**, *36*, 25–32.
47. Chamkha, A.J.; Aly, A.M.; Mansour, M.A. Similarity solution for unsteady heat and mass transfer from a stretching surface embedded in a porous medium with suction/injection and chemical reaction effects. *Chem. Eng. Commun.* **2010**, *197*, 846–858. [CrossRef]
48. Sharidan, S.; Mahmood, T.; Pop, I. Similarity solutions for the unsteady boundary layer flow and heat transfer due to a stretching sheet. *Int. J. Appl. Mech. Eng.* **2006**, *11*, 647–654.
49. Mukhopadhyay, S.; Gorla, R.S.R. Unsteady MHD boundary layer flow of an upper convected Maxwell fluid past a stretching sheet with first order constructive/destructive chemical reaction. *J. Nav. Archit. Mar. Eng.* **2012**, *9*, 123–133. [CrossRef]
50. Bibi, M.; Rehman, K.U.; Malik, M.Y.; Tahir, M. Numerical study of Unsteady Williamson fluid flow and heat transfer in the presence of MHD through a permeable stretching surface. *Eur. Phys. J. Plus* **2018**, *133*, 154. [CrossRef]
51. Kebede, T.; Haile, E.; Awgichew, G.; Walelign, T. Heat and mass transfer in unsteady boundary layer flow of Williamson nanofluids. *J. Appl. Math.* **2020**, *2020*, 1890972. [CrossRef]
52. Khan, M.; Azam, M. Unsteady heat and mass transfer mechanisms in MHD Carreau nanofluid flow. *J. Mol. Liq.* **2017**, *225*, 554–562. [CrossRef]